Remote Sensing of Environment 147 (2014) 133–144

Contents lists available at ScienceDirect

Remote Sensing of Environment

journal homepage: www.elsevier.com/locate/rse

Evaluating sub-pixel offset techniques as an alternative to D-InSAR for monitoring episodic landslide movements in vegetated terrain

A. Singleton [a,*], Z. Li [a,b], T. Hoey [a], J.-P. Muller [c]

[a] School of Geographical and Earth Sciences, University of Glasgow, University Avenue, Glasgow G12 8QQ, UK
[b] School of Civil Engineering and Geosciences, Cassie Building, Newcastle University, Newcastle upon Tyne NE1 7RU, UK
[c] Imaging Group, Mullard Space Science Laboratory, Department of Space and Climate Physics, University College London, Holmbury St. Mary RH5 6NT, UK

ARTICLE INFO

Article history:
Received 1 August 2013
Received in revised form 13 December 2013
Accepted 7 March 2014
Available online 28 March 2014

Keywords:
Synthetic Aperture Radar (SAR)
Differential SAR interferometry (D-InSAR)
SAR sub-pixel offsets
Time-series analysis
TerraSAR-X Spotlight
TerraSAR-X Stripmap
Envisat
Corner reflectors (CR)
Three Gorges region (China)
Slow-moving landslides

ABSTRACT

Spaceborne Synthetic Aperture Radar (SAR) sensors obtain regular and frequent radar images from which ground motion can be precisely detected using a variety of different techniques. The ability to measure slope displacements remotely over large regions can have many uses, although the limitations of the most commonplace technique, differential InSAR (D-InSAR), must be considered prior to interpreting the final results. One such limitation is the assumption that different rates of movement over a given distance cannot exceed a threshold value, dependent upon the pixel spacing of the SAR images and the radar wavelength. Characteristic features of landslides (i.e. the sharp boundary between stable/active ground and the range of temporally-variable velocities) can exhibit high spatial displacement gradients, breaking a fundamental assumption for reliable D-InSAR analysis. Areas of low coherence are also known to hinder the exploitation of InSAR data. This study assesses the capability of TerraSAR-X Spotlight, TerraSAR-X Stripmap and Envisat Stripmap images for monitoring the slow-moving Shuping landslide in the densely vegetated Three Gorges region, China. In this case study, the episodic nature of movement is shown to exceed the measurable limit for regular D-InSAR analysis even for the highest resolution 11-day TSX Spotlight interferograms. A Sub-Pixel Offset Time-series technique applied to corner reflectors (SPOT-CR) using only the SAR amplitude information is applied as a robust method of resolving time-varying displacements, with verifiable offset measurements presented from TSX Spotlight and TSX Stripmap imagery. Care should be exercised when measuring potentially episodic landslide movements in densely vegetated areas such as the Three Gorges region and corner reflectors are shown to be highly useful for SPOT techniques even when the assumptions for valid D-InSAR analysis are broken. Finally the capability to derive two-dimensional movements from sub-pixel offsets (in range and along-track directions) can be used to derive estimates of the vertical and northwards movements to help infer the landslide failure mechanism.

1. Introduction

Satellite radar imagery has been recognised as a powerful tool for measuring surface motions over large regions and offers the capability to remotely monitor unstable slopes (Rott, Scheuchl, Siegel, & Grasemann, 1999; Tofani, Segoni, Catani, & Casagli, 2010). In the best cases of landslide management, Early Warning Systems (EWS) have been developed and employed to minimise harm and loss. The nature of EWS and the landslide risk is strongly dependent upon landslide type, which is often classified by the initial mechanism of motion and the associated velocity (Cruden & Varnes, 1996). Whilst rapid landslides are the most dangerous, deep and slow landslides are capable of destroying buildings and infrastructure particularly on reactivated ancient landslide deposits (Sassa, Picarelli, & Yueping, 2009).

A well-developed EWS should include various elements such as understanding the local knowledge of risks, communicating timely and reliable warnings, and building local capacity to respond to warnings (UN-ISDR, 2004). However, one other technical component involves monitoring the hazard(s) which requires: (i) detection; (ii) rapid mapping; (iii) characterisation; and, (iv) long-term monitoring of landslides (Tofani et al., 2010). The generic benefits of using remote sensing data are well known, and a sub-report from the European SAFELAND Project (Stumpf, Kerle, & Malet, 2010) compares the merits of numerous remote sensing techniques for monitoring different types of landslides. Airborne LiDAR surveys can provide useful data in terms of spatial resolution, precision and the capacity to measure a variety of displacement rates, although the cost and logistics required for regular repeat acquisitions are barriers for its routine use. Synthetic Aperture Radar (SAR) images from the most recent generation of SAR

* Corresponding author.
E-mail addresses: a.singleton.1@research.gla.ac.uk (A. Singleton), zhenhong.li@newcastle.ac.uk (Z. Li).

http://dx.doi.org/10.1016/j.rse.2014.03.003
0034-4257/

satellite sensors (e.g. TerraSAR-X and COSMO SkyMed) can acquire regular data (up to every 4 days), over regional areas (e.g. 10–1000 km^2), at a high resolution (up to 1 m ground resolution) and in the case of slow-moving landslides (i.e. several metres per year; Cruden & Varnes, 1996), can meet the four requirements of landslide monitoring mentioned above. Whilst the repeat interval may not be short enough to provide timely warnings to vulnerable populations, it is possible to detect individual landslide accelerations over large regions and then direct monitoring equipment to areas at risk. The ability to make numerous point measurements of displacement over the landslide body can not only identify and map the actively deforming slopes (significantly reducing uncertainty in landslide inventory maps; e.g. Cascini, Fornaro, & Peduto, 2010), but also help to characterise the landslide mechanism (Tofani, Raspini, Catani, & Casagli, 2013). Further interpretations of landslide processes can then be inferred when comparing a time-series of displacement with potential triggering factors such as rainfall, seismicity and site-specific factors such as fluctuating reservoir water-levels (e.g. Tolomei et al., 2013). Finally, historic landslide movements can be measured from SAR satellite imagery using archived data scenes.

Whilst differential InSAR (D-InSAR) analysis is capable of mapping and measuring landslide movements, a major limitation is dense vegetation which can lead to rapid decorrelation between SAR acquisitions even for the highest resolution TSX Spotlight image mode with a revisit time of 11-days. Episodic and spatially variable landslide movements can also lead to decorrelation between SAR acquisitions when the spatial displacement gradient is exceeded. Determining the cause of decorrelation is often difficult and whilst time-series InSAR techniques have been developed to identify slowly decorrelating pixels in vegetated areas (e.g. Hooper, 2008; Hooper, Segall, & Zebker, 2007), resolving episodic and time-varying displacements remains a difficult task.

In this paper, Sub-Pixel Offset Time-series techniques applied to corner reflectors (SPOT-CR) using frequently acquired SAR images from a variety of sensors are quantitatively evaluated and compared for landslide monitoring. The measured landslide displacements are then used to help judge the suitability of using more precise D-InSAR time-series techniques in situations where assumptions of conventional D-InSAR analyses can be broken by the characteristic features of landslides (i.e. the sharp boundary between stable/active ground, the non-linear nature of the displacements and the range of temporally-variable velocities). The benefits and limitations of SPOT-CR techniques are assessed for studying landslides on densely vegetated slopes and their ability to monitor spatially large 2-dimensional movements using the installed corner reflectors is shown to infer a possible failure mechanism of the Shuping landslide within the Three Gorges region, China.

2. Investigating landslides using SAR observations

D-InSAR has been employed to monitor the slow motion of many landslides and compared to (typically sparse) GPS point measurements (e.g. Akbarimehr, Motagh, & Haghshenas-Haghighi, 2013; Wen-Yen, Chih-Tien, Chih-Yuan, & Jyun-Ru, 2012), D-InSAR techniques are especially useful for providing spatially continuous coverage of surface displacement which can help define the boundaries of active landslides (Yin, Zheng, Liu, Zhang, & Li, 2010). Rott et al. (1999) used D-InSAR to examine a slow moving landslide (up to 4 cm/yr) in the Austrian Alps highlighting the inter-annual variability of displacements, and the limitations of D-InSAR techniques for landslide monitoring were proposed for the first time. Over the last decade, the number of InSAR applications to landslide studies has grown significantly following initial studies (e.g. Berardino et al., 2003; Fruneau, Achache, & Delacourt, 1996; Strozzi et al., 2005), with comprehensive overviews of interferometric SAR (InSAR) techniques for landslide studies presented by Colesanti and Wasowski (2006) and Rott and Nagler (2006) for sensors such as Envisat/ASAR and RADARSAT. However, it should be noted these reviews pre-date the launch of the most recent commercial SAR sensors. Rott (2009) provides a slightly updated summary with reference to the TerraSAR-X and COSMO SkyMed satellites.

Despite the advantages of D-InSAR methods these continue to have limitations that should always be considered, such as geometric decorrelation, temporal decorrelation, atmospheric artefacts, scale constraints, a limit on the spatial displacement gradient, geometric distortions and a 1-dimensional Line-of-Sight (LOS) measurement sensitivity (Colesanti & Wasowski, 2006) and assumptions of linearity in the displacement process. A range of techniques have been developed to help minimise some of these effects (e.g. time-series analysis to estimate various phase components; Berardino, Fornaro, Lanari, & Sansosti, 2002; Ferretti, Prati, & Rocca, 2001, using external data to reduce atmospheric path delays; Foster et al., 2013; Li, Fielding, Cross, & Muller, 2006; Li, Muller, Cross, & Fielding, 2005; Onn & Zebker, 2006), although fundamental theoretical constraints still exist. It has been suggested that the inherent limitations of SAR data, coupled with the complexity of landslides, may be insufficiently appreciated which results in the misrepresentation of landslide measurements (Peduto, Cascini, & Fornaro, 2010). Consequently, end-users can lack confidence in these remotely-sensed results unless verified with ground data (thereby negating some of the benefits of using remotely collected data).

To illustrate a potential problem with D-InSAR analysis, consider the loss of coherence which often occurs between two time-adjacent SAR acquisitions in a densely vegetated region. This might be wrongly interpreted to result from temporal decorrelation when the real reason was a landslide movement exceeding the spatial displacement gradient. Subsequently, any D-InSAR time-series technique spanning this fast event would erroneously underestimate the landslide displacement. Such a scenario is shown to occur in the Three Gorges and motivates this research to find a complimentary technique to extract verifiable landslide measurements from SAR images.

A range offset map from SAR pixel offset methods contains the same information as a differential interferogram (Yun, Zebker, Segall, Hooper, & Poland, 2007) and being less restricted by the assumption of a low spatial displacement gradient, provides a useful comparison with InSAR results. Past studies using SAR pixel offset methods have been dominated by co-seismic and glacial applications, due to the widespread decorrelation in conventional interferograms from high deformation gradients across ruptured faults or rapidly changing ice surfaces. As such, accurate fault traces have been revealed using pixel offset techniques (e.g. Funning, Parsons, Wright, Jackson, & Fielding, 2005; Jónsson et al., 2002; Li, Elliott, et al., 2011; Michel, Avouac, & Taboury, 1999) along with the capability to remotely measure glacier/rock glacier flow (e.g. Haug, Kääb, & Skvarca, 2010; Quincey et al., 2005; Scambos, Dutkiewicz, Wilson, & Bindschadler, 1992).

To date, only a small number of studies have used pixel offset techniques for monitoring slope movements, the majority using optical imagery from airborne and spaceborne platforms (Debella-Gilo & Kääb, 2011; Delacourt, Allemand, Casson, & Vadon, 2004; Kääb, 2002; Leprince, Berthier, Ayoub, Delacourt, & Avouac, 2008; Wangensteen et al., 2006; Yamaguchi, Tanaka, Odajima, Kamai, & Tsuchida, 2003). The sensitivities of normalised cross-correlation were considered by Delacourt et al. (2004) and Debella-Gilo and Kääb (2011) which include: (i) noise in the images; (ii) rotation/shearing between the images to be correlated; and (iii) the relationship between the pixel size and the precision of measurements. However, optical images can only be used to assess purely horizontal movements (north–south and east–west directions) without consideration of the vertical component. A sub-pixel offset technique was first applied to (TerraSAR-X Spotlight) SAR data by Li, Muller, et al. (2011) with promising results for monitoring the Shuping landslide, although only 4 sets of measurements were shown in the paper (corresponding to 4 offset pairs). This study attempts to recover landslide movements from

TerraSAR-X data with a temporal resolution of up to every 11 days over a time period of 15 months.

3. Landslides in the Three Gorges region

Landslides, mainly deep and slow-moving, are the most frequent and widespread geohazard in the Three Gorges region, predominantly caused by high slope gradients, lithological susceptibilities, heavy summer rainfall and human activities (Liu et al., 2004). Over the last decade, the construction of the Three Gorges project (TGP) has created a 600 km long reservoir with a bi-annually fluctuating water level (range ≈ 25 m) which has been shown to reactivate ancient landslides (Wang, Zhang, et al., 2008). The Three Gorges were formed by incision along narrow fault zones of massive limestone mountains interbedded with siltstone, shale and mudstone (Wang, Harvey, et al., 2008), although between the gorges the lithologies are much less resistant. Dominated by weathered mudstones, these inter-gorge areas favour river bank erosion, terrain dissection and the development of slow-moving slope failures (Liu et al., 2004).

This study focuses on the Shuping landslide located towards the eastern end of the Three Gorges (Fig. 1), the toe of which is connected to the Yangtze River. The Shuping landslide was selected as a case study and regular SAR data were commissioned in three different image modes over the landslide over the same time period. These data allow robust comparisons between data modes and the application of D-InSAR or sub-pixel offset techniques. The landslide is densely vegetated with orange trees, representative of the majority of hillslopes in the Three Gorges region, which makes the application of D-InSAR techniques very difficult. The north facing landslide orientation also makes it insensitive to LOS measurements. Independent of this study, corner reflectors have been installed over the landslide which aid the analysis of SAR data.

Previous studies that have monitored the Shuping landslide using D-InSAR techniques have yielded highly varied results. Fu, Guo, Tian, and Guo (2010) used 12 corner reflectors installed over the landslide to obtain a single measurement of displacement between September 2005 and March 2006 using Envisat data. Good agreement with GPS measurements was reported, although this result did not cover the months of April–June where the fastest movements are normally observed (and when the assumptions for reliable D-InSAR analysis are most likely to be broken).

Extensometer measurements over the time period of September 2005 and June 2007 show minimal displacements until around May–June 2007 when there is a rapid increase of ~0.4 m in the accumulated movements up to June 2007 (Wang et al., 2013). Whilst recognising the different vectors of measurement sensitivity, this contradicts the results of Xia (2010) who used the same 12 corner reflectors to calculate a time-series of displacement over the same time period, presenting very linear rates of downwards movement for all points.

This landslide has been divided into eastern and western parts with the eastern block (also known as Block 1) shown to be most active (Wang, Zhang, et al., 2008). The motion of Block 1 has been recorded primarily using extensometers from 2004 until 2010 (Wang, Zhang, et al., 2008; Wang et al., 2013) and these results display high spatial variability along with a stepped behaviour in time. Particularly using the longest record of movement, from August 2004 until May 2010, the periods of greatest movement have been suggested to relate to the drawdown of the Three Gorges Reservoir (Wang, Zhang, et al., 2008). Liao, Tang, Wang, Balz, and Zhang (2012) used Persistent Scatterer (PS) interferometry with TerraSAR-X Stripmap data to show movements up and down in the LOS direction in the order of ±5 mm between February 2008 and January 2010 which is unusual given that these measurements are an order of magnitude lower than the extensometer data. The highly non-linear velocity trend revealed by in-situ measurements and the disparities between previous D-InSAR studies prompts further analysis of the Shuping landslide using SAR data.

4. Methods

4.1. Data

The availability of 36 commissioned TerraSAR-X (TSX) Spotlight SAR images, 23 TSX Stripmap images as well as 17 Envisat Stripmap images all covering the same Shuping landslide (and significantly overlapping in time; see Fig. 1 and Supplementary material Table S1), also enables comparison of D-InSAR and SPOT-CR techniques which both aim to remotely monitor the landslide without the use of ground data. All results presented below were produced using the SARscape® software package (SARMAP, 2012), which includes an interferometry module capable of processing the above image modes along with an amplitude tracking tool for calculating sub-pixel offsets.

4.2. Maximum spatial displacement gradients and coherence analysis

One major limitation of D-InSAR techniques is their inability to measure high spatial gradients of rapid deformation. To observe

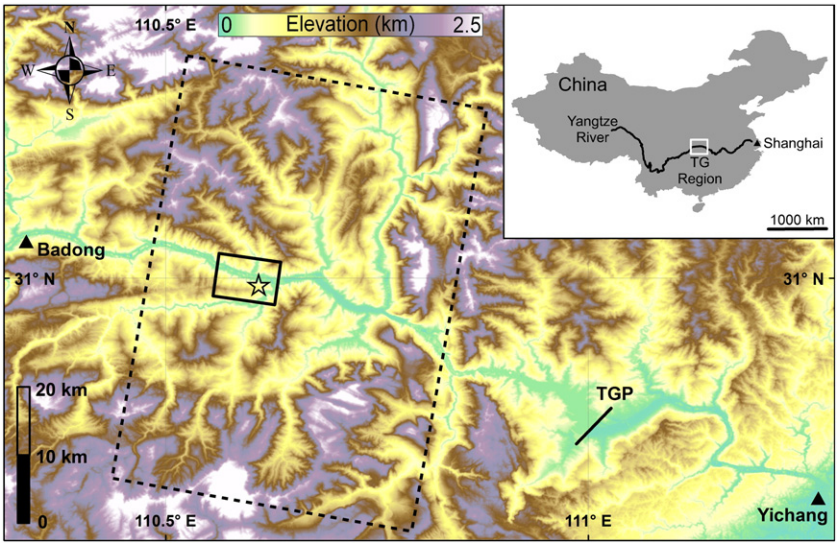

Fig. 1. Elevation of the eastern Three Gorges (TG) region. The star indicates the site of the Shuping landslide, ca. 45 km upstream of the Three Gorges Project (TGP). TSX Spotlight data coverage is shown by the solid box and TSX Stripmap data coverage is given by the dashed box. Envisat data covers the whole map.

interferometric fringes without ambiguity, the maximum displacement between two neighbouring pixels in a wrapped interferogram must not exceed λ / 2 (Massonnet & Feigl, 1998), with wavelengths (λ) typically in the order of ~30–300 mm. However, from the viewpoint of phase unwrapping, the maximum displacement gradient should be less than 0.5 fringes per pixel (Jiang, Li, Ding, Zhu & Feng, 2011; Spagnolini, 1995) making the limit of displacement between neighbouring pixels λ / 4. As such, D-InSAR has most commonly been applied to deformation phenomena measureable within these limits, such as very slow moving landslides, city subsidence, volcanoes and far-field earthquake deformation patterns. This theoretical limit does not consider noise in the radar observations caused by decorrelation effects (Zebker, Rosen, & Hensley, 1997) and hence reduces the maximum realistic measureable displacement gradient (Baran, Stewart, & Claessens, 2005; Jiang et al., 2011). It is therefore practically impossible to derive measurements of fast-moving phenomena with sharp boundaries between stable and moving areas such as glaciers, co-seismic deformation near faults and landslides moving beyond a threshold limit. The capability of D-InSAR to measure such movements is primarily determined by the pixel spacing and the wavelength of the SAR sensor.

The limits on the spatial displacement gradient are the theoretical maxima when the radar observations are unaffected by noise. Decorrelation between SAR acquisitions can be a major problem in the use of D-InSAR techniques particularly in densely vegetated regions (Ahmed, Siqueira, Hensley, Chapman, & Bergen, 2011) such as the Three Gorges. To assess the decorrelation effects, interferometric coherence was analysed for all three image modes. Differential interferograms were generated with a multi-look factor of 2 applied in both range and azimuth, and the topographic phase component was removed using the ASTER GDEM v2, a product of METI and NASA, with a RMSE of 12.1 m compared to 121 GPS benchmarks in the Three Gorges area (Li et al., 2012). To measure the interferometric coherence, a sample estimate using a 9 × 9 window was employed for an area of 5 km^2 adjacent to but excluding the landslide body, from which a mean coherence could be obtained. Seasonal patterns were assessed by plotting the mean coherence for every 11-day (TSX) or 35-day (Envisat) pair over time. Effects of the perpendicular baselines were considered by plotting the mean coherence for the same pairs with respect to the baseline and to assess the temporal decorrelation, the mean coherence for all pairs with a baseline less than 25 m (TSX data) or 50 m (Envisat data) was plotted with respect to the time interval between image acquisitions (Fig. 2). For the generation of the final interferograms, a spectral shift filter accounting for the difference in incidence angles between master and slave images (Gatelli et al., 1994) was applied, along with a Doppler filter to remove the non-overlapping azimuth spectra between the master and slave images.

4.3. Sub-pixel offset techniques

Although less precise than conventional InSAR methods, pixel offset techniques using SAR amplitude images can overcome the D-InSAR limitation on the spatial displacement gradient and are far more robust (not requiring phase unwrapping, not strongly limited to regions of high coherence and significantly less affected by atmospheric water vapour due to an independence on the use of phase values). Additionally, pixel offset data can provide complimentary information since conventional interferograms are only sensitive to displacements in the sensor's LOS direction (Michel et al., 1999). Using just two images acquired at different times, displacement vectors can be measured in the sensor look direction (range) as well as the satellite flight (along-track, or 'azimuth') direction. The 2-dimensional measurements are obtained by measuring the row and column offsets between the two acquisitions at defined intervals in range/azimuth in order to generate sufficient coverage of offset measurements (Pathier et al., 2006).

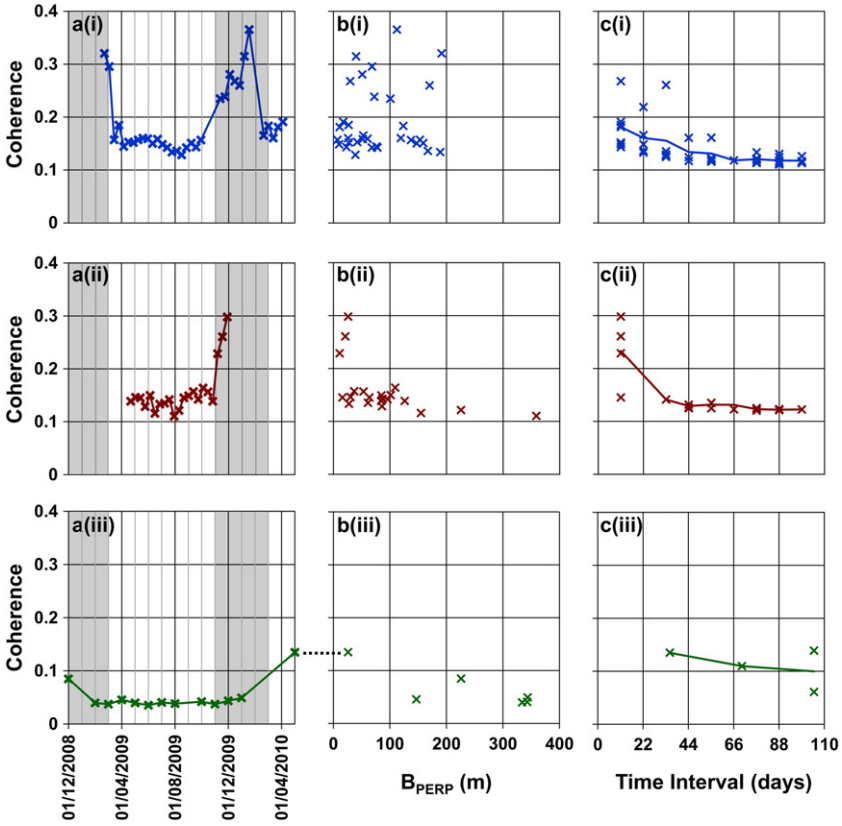

Fig. 2. (a) Coherence of temporally-adjacent SAR images showing highest values between November and February each year. (b) Coherence of 11-day (TSX) or 35-day (Envisat) interferograms plotted against perpendicular baseline showing no significant patterns. (c) Coherence of interferograms with respect to time interval showing a decline by ~30 days. (i) TSX Spotlight data (ii) TSX Stripmap data (iii) Envisat data.

SPOT-CR techniques are capable of measuring more spatially variable movements than D-InSAR although the results from pixel offset methods are highly dependent upon the various processing parameters (notably the cross-correlation window size and oversampling factor) which should be carefully tuned with regard to the scale of the deformation feature(s) and the pixel size of the SAR images (Bechor & Zebker, 2006; Yun et al., 2007). Consequently, the size of the moving window should be large enough to maximise the signal-to-noise ratio whilst minimising the spatial velocity gradient. The search area size must also be large enough to include the fastest moving distance whilst minimising the computational cost of the process (Debella-Gilo & Kääb, 2011). Following an approach outlined by Yun et al. (2007), the cumulative distribution for an area of 2 km^2 (adjacent to the landslide site and assumed to be stable) was analysed with a combination of different parameters. Visual inspection from these tests provides a heuristic way of tuning the moving window size and the oversampling parameters, considering the data characteristics and the phenomenon under study. However, contrary to Yun et al. (2007), no piecewise linear fit was used to exclude any offset value since valid landslide offsets would be concentrated in one tail of the distribution when considering the stable ground also within the offset map.

Prior to generating the sub-pixel offset measurements, SAR images were aligned using a simple translational shift based on the orbital data and the digital elevation model. A standard normalised cross-correlation procedure based on the optimal window size and oversampling factor was then applied without any filtering in any part of the processing, and the final offset values used to generate the time-series curves were taken as the mean from a small window of 10 × 10 pixels at various locations around the landslide. The same window position in rows/columns was used to extract measurements from every subsequent slave image for the time-series.

5. Results and analyses

5.1. Maximum spatial displacement gradients and coherence analysis

For the three different image modes employed in this study, the spatial displacement gradients were considered. Table 1 displays the displacement gradients for an interferogram produced at the original SLC resolution and when considering a small multi-look factor of two. The pixel size controls the maximum measurable displacement and, even for the highest resolution TSX Spotlight imagery, it would not be possible to measure a difference in the displacement between image acquisitions of more than 0.12 m (or 0.06 m after multi-looking) over a distance of 10 m. Despite the slightly longer wavelength of Envisat data, the greater pixel size is a significant disadvantage for measuring spatially variable movements over short distances.

The results of the coherence analysis are presented in Fig. 2. The coherence between temporally-adjacent SAR images over the time period of available acquisitions for all image modes (Fig. 2: left hand column) is low throughout the 1.5 years, although a consistent seasonal pattern is shown for the TSX imagery whereby coherence increases between November and February each year. Given the sensitivity of radar backscatter to the dielectric effects of changing the surface moisture content (Smith, 2002), the seasonal coherence pattern could be attributable to the heavy summer rainfall after comparing the coherence trends with the mean monthly rainfall values for the winter (~19 mm/month for November–February) and the rest of the year (~100 mm/month for March–October). The seasonality in coherence and rainfall may also be interrelated with the dense orange trees in the area since the canopy reflectance can change significantly over the year even if the orange trees are evergreen (Dzikiti et al., 2011).

Despite its shorter wavelength, the TSX data display higher coherence than the Envisat data due to its higher resolution and shorter repeat interval. Coherence for each 11-day (TSX) or 35-day (Envisat) interferogram with respect to the perpendicular baseline (Fig. 2: middle column) shows no definitive trend over the relatively short range of baselines (up to 400 m), and the coherence values > 0.2 are from interferograms created in the dry winter period. The right hand column of Fig. 2 shows coherence for all interferograms with a baseline of less than 25 m (TSX) or 50 m (Envisat) in relation to the time-interval between acquisitions. A relatively fast fall in coherence is seen with the TSX data until the interval exceeds ~33 days where it remains at a constant non-zero level. This constant value is considered to represent the natural bias in estimating the coherence correlation magnitude (Touzi, Lopes, Bruniquel, & Vachon, 1999). The almost complete loss of coherence beyond 33 days also explains why no significant seasonal coherence pattern is observed from the Envisat data. The low coherence throughout the time period suggests that the maximum measurable spatial displacement gradient is below the theoretical values presented in Table 1.

Table 1
Displacement gradients (m/m) for original resolution interferograms and for interferograms with a small multi-look factor of 2. The data used in these calculations are shown in the Supplementary material (Table S1). Multiply these values by the distance between two points to calculate the maximum detectable difference in the rates of displacement.

Sensor/image mode	Displacement gradient (DG)	DG after multi-looking (using a small factor of 2)
TerraSAR-X/Spotlight	0.01177	0.00589
TerraSAR-X/Stripmap	0.00394	0.00197
Envisat ASAR/Stripmap	0.00070	0.00035

5.2. D-InSAR analysis

To remotely monitor landslides with high precision, the optimal approach would use high coherence interferograms with minimal geometric distortions which cover the whole time period. Given that the shortest time intervals gave the best coherence, every 11-day TSX Spotlight pair was processed using a Goldstein filter (Goldstein & Werner, 1998) prior to geocoding. Fig. 3 shows three of these (wrapped) interferograms for adjacent 11-day intervals. The landslide boundary is indicated by the sharp colour changes as shown by the black line, and this boundary is consistent over the 33-day period (3 × 11-day interferograms).

Assuming a purely translational failure mechanism parallel to the slope surface, sliding velocities can be projected into the downslope sliding direction (e.g. Hilley, Bürgmann, Ferretti, Novali, & Rocca, 2004) although using a scaling factor impacts on the precision of measurements (Colesanti & Wasowski, 2006). The SAR geometry is typically incapable of measuring translational movements on ascending or descending orbits for slope aspects close to 0° and 180° (Cascini et al., 2010) and for Envisat ascending data a scaling factor threshold of 3.3 was used to select suitable 'projectable' PS points (Cascini et al., 2013). Projection of the TSX Spotlight D-InSAR data in Fig. 3 was not undertaken primarily due to the high scaling factor (9.8 for the north-facing Shuping landslide).

In Fig. 3 an increase in the fringe rate can also be observed from left to right, which relates to an increase in the landslide movement over each interval. However, Fig. 3b and c shows a loss of coherence particularly towards the head of the landslide that is most likely due to the displacements exceeding the maximum measurable limit of 0.00589 m/m (see Table 1). The sole use of these TSX Spotlight images (or lower resolution X-band or C-band SAR images) for any D-InSAR time-series analysis would subsequently underestimate landslide displacement and a technique is required to verify whether this coherence is lost due to the fast landslide movement or other factors.

5.3. Sub-pixel offset observations

Over a completely stable area, the offset value should be randomly distributed around a mean of zero, although with small moving window

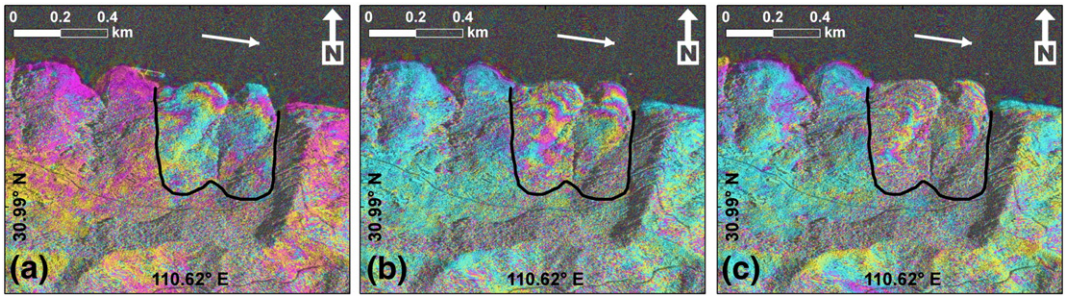

Fig. 3. Wrapped, 11-day TSX Spotlight interferograms covering the time periods: (a) 09/05/09–20/05/09; (b) 20/05/09–31/05/09; and (c) 31/05/09–11/06/09. Colour cycles represent modulo-2π phase changes and therefore each cycle represents ~0.016 m of displacement in the radar Line-of-Sight (LOS) direction. Assuming the main landslide movement is northwards (downslope towards the river), the LOS direction is perpendicular to the landslide direction and must be most sensitive to vertical surface changes, shown by the unit vector defining the look direction of the TSX Spotlight imagery $u = [d_E\ d_N\ d_U] = [-0.68\ 0.12\ -0.72]$ (positive up, left-handed coordinate system). This shows only around 12% of possible north–south displacement is recorded by TSX Spotlight D-InSAR data. The white arrow shows the flow direction of the Yangtze River.

sizes and no oversampling, the distribution of values is determined by the size of the moving window (Fig. 4) due to spurious correlation. As the oversampling factor increases for the small window sizes, the range of possible offset values increases to eradicate the step-like behaviour of the cumulative distribution, but the linear trend shows no concentration around zero. For a window size of 32 × 32 pixels, ~75% of the offset values are between ±0.5 pixel units and the oversampling factor was increased until no observable improvement is seen (an oversampling factor of 16 is identical to an oversampling factor of 24). As the window size and oversampling factors are increased, the results improve but the processing time should also be considered. For example, doubling the window size from 32 × 32 pixels to 64 × 64 pixels increases the processing time for each offset pair from 01:41 h to nearly 05:37 h (detailed processing timings shown in Supplementary material Table S2). Given the associated times for generating one offset measurement using different parameters, the final selection of a 32 × 32 pixel window size and an oversampling factor of 16 was deemed preferable.

Following the processing of the first offset pair, the correlation values associated with each offset measurement (Fig. 5) show that points with very high correlations (>0.9) are distributed across the landslide in positions which correspond to the corner reflector locations. Given the significant contrast in the radar backscatter between the corner reflectors and the natural terrain, these points result in a very high cross correlation value when they are within the total area covered by the moving window used in the calculation. Following the numbering scheme displayed on the right of Fig. 5, it is clear that most are within the landslide boundary, although a number of points are situated outside the landslide on ground that is assumed to be stable which can then help identify the potential noise level of the offset measurements.

5.4. Results of Sub-Pixel Offset Time-series techniques applied to corner reflectors (SPOT-CR)

A final step in the processing strategy considered how to generate a time-series of measurements. The two simplest approaches are to: (i) use the same master image with subsequent slave images; and, (ii) process every 11-day offset pair to generate a cumulative time-

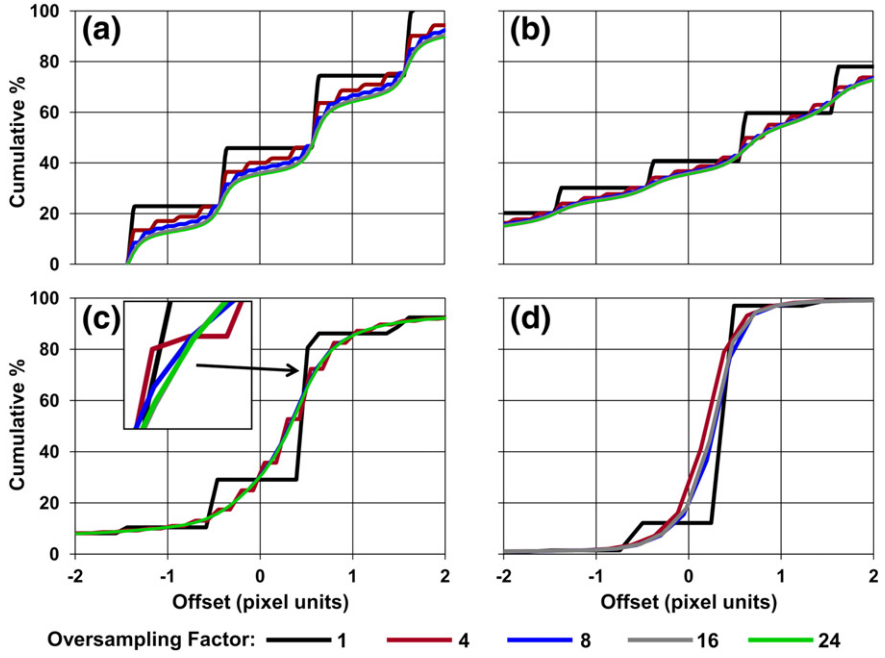

Fig. 4. Cumulative percentage of TSX Spotlight sub-pixel offset values in the azimuth direction over a stable area of ground (1.75 km^2) adjacent to the landslide. This is plotted for different pixel-oversampling factors and also different cross-correlation window sizes: (a) 4 × 4, (b) 8 × 8, (c) 32 × 32, and (d) 64 × 64. A window size of 16 × 16 was also assessed (Supplementary material Fig. S1). The final parameter set used a window size of 32 × 32 since this results in >80% of the area being characterised with values around zero. A larger window size increases precision but the processing time is significantly longer (see Supplementary material Table S2). An oversampling factor of 16 was chosen, above which no improvement is observed as shown by the inset of Fig. 4c.

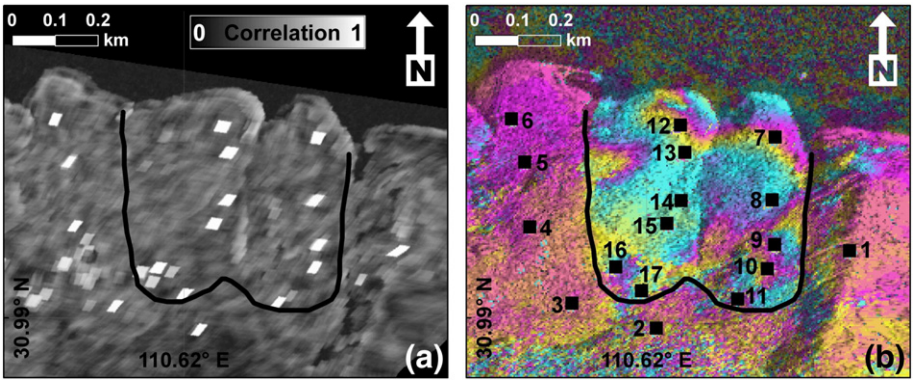

Fig. 5. (a) The value of peak correlation used for the TSX Spotlight offset measurements (11-day pair, 21st Feb–4th Mar 2009, showing the minimum temporal decorrelation). The high correlations (the white areas) are caused by a high-contrast feature (mostly corner reflectors) within the cross-correlation window. The same features are observed for the TSX Stripmap offset measurements. (b) The numbering of corner reflectors used to extract time-series of displacement in Fig. 7(a–d), overlain on an interferogram showing the landslide boundary (11-day pair, 9th May–20th May 2009). Point 1 is outside the landslide and used as the reference for all other points. Points 2–6 are also outside the landslide boundary. Points 7–11 ascend up the east part of the landslide. Points 12–17 ascend up the west part of the landslide. Point 3 was excluded from analysis after results suggested it had unnaturally shifted (see Supplementary material Fig. S4).

series of displacement. The first of these possibilities is preferred since the temporal decorrelation from the corner reflector points is believed to be very small, and this strategy ensures that errors in each offset measurement is independent from the results of previous image pairs. For example using time-adjacent pairs, the first measurement would be the result of just one offset pair whereas the last measurement would be calculated as the sum of all previous offset measurements. An alternative to both the above strategies is to create a small-baseline (SBAS) network of offset pairs, similar to that proposed by Casu, Manconi, Pepe, and Lanari (2011). Using Envisat data, Casu et al. (2011) attempted to reduce the perpendicular baselines of the offset pairs which influenced the amount of reliable measurements generated. When considering the TSX data used here, no significant dependence upon the perpendicular baseline is observed (Fig. 6) most likely due to the consistently short perpendicular baseline values which never exceed 300 m. Additionally, no significant decay in the amount of reliable pixels is observed over time and so the benefit of inverting a SBAS network of offset maps to generate a time-series of displacement is limited. The simplest approach ((i) above) of using one constant master image for all the offset pairs therefore meets the requirements of this investigation.

The offset time-series graphs from TSX Spotlight and Stripmap data (Fig. 7) show a significant step in landslide movement in both the range and azimuth directions towards the end of May and the start of June. Movements of more than 0.1 m recorded towards the head of the landslide over an 11-day period further explain the loss of coherence from the interferograms presented in Fig. 3. Additionally, considering the curves related to the points outside the landslide boundary, it is noted that the noise in the azimuth direction measurements exceeds that in the range direction, a result that is assumed to be caused by the larger azimuth pixel spacing. Additionally, the variability in subsequent offset values from the Stripmap data is greater than the Spotlight data which is another likely consequence of the larger pixel spacing.

Considering the topographical location of the corner reflectors, a strong association is found between elevation and the range displacement. Displacement in the LOS (which includes a vertical component of movement) is up to ten times greater towards the head of the landslide which may reflect the failure mechanism. No such topographic dependence is shown in the azimuth offset results. These patterns in both range and azimuth are very consistent between the Spotlight and Stripmap data and given the independence of the datasets, the duplicate measurements over the same time period validate the results without the requirement for ground data. Confidence in the SPOT-CR results is boosted by a qualitative comparison to extensometer data over the same time period (Wang et al., 2013). The maximum step-like displacement of ~0.5 m occurred in May 2009 before stabilising for the remainder of the year. Despite this extensometer measurement being taken at the eastern boundary of the landslide, the magnitude and timing of movements recorded by the extensometer closely follow the results presented here. Additionally, the magnitude and

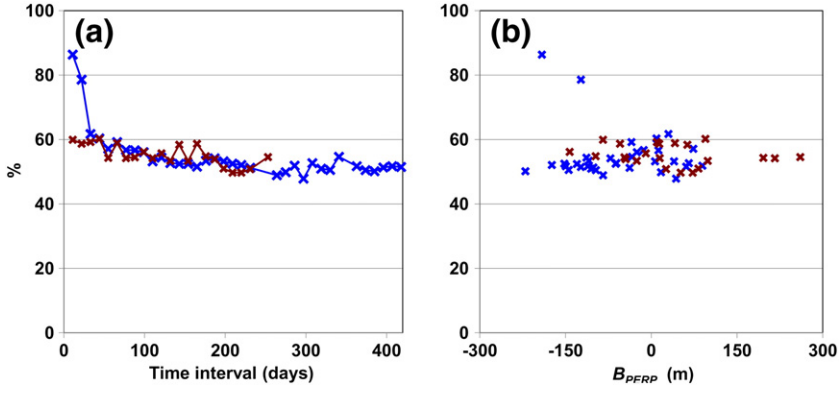

Fig. 6. Percentage of pixels with a correlation above an arbitrary value of 0.25 with respect to (a) the time interval between master and slave image and (b) the perpendicular baseline. This is shown for both the TSX Spotlight offsets (blue) and TSX Stripmap offsets (red). No obvious deterioration is seen with respect to increasing perpendicular baselines which contrasts the pattern shown by Envisat data in Casu et al. (2011), most likely due to the far smaller range in perpendicular baselines of the TSX data.

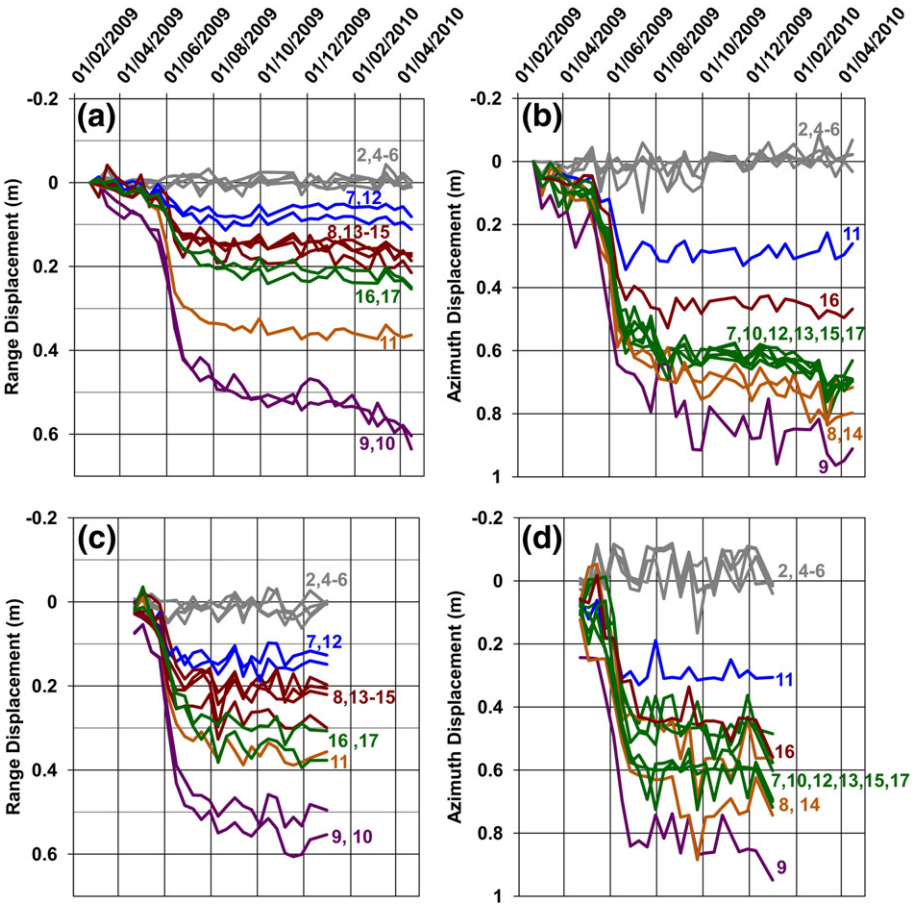

Fig. 7. Offset displacement of the corner reflectors. (a–b) Range and azimuth offsets measured from TSX Spotlight data. (c–d) Range and azimuth offsets measured from TSX Stripmap data. The positive scale is away from the sensor in range dimension and the reverse along-track direction (i.e. predominantly northwards) in azimuth dimension.

linearity of repeated GPS measurements closely follow the range offset results for the GPS survey period August 2009–April 2010 (Liao, Zhang, & Balz, 2013).

5.5. Accuracy assessment of SPOT-CR results

An assessment of the offset errors is undertaken using two independent offset pairs significantly overlapping in time. The offsets were measured between the first and penultimate available image, and compared to offsets between the second and last image (~9 months for TSX Spotlight and ~5 months for TSX Stripmap data). Since using these data to assess errors assumes that the displacements in these two time periods are equal, the two master images were chosen at the start of August since this is when the landslide velocity had significantly reduced. The differences between offset measurements from these overlapping pairs for both the TSX Spotlight and TSX Stripmap imagery are shown in Table 2. Using the corner reflector points to generate the offset measurements, the RMS errors are all less than 0.038 m and 0.071 m in the range and azimuth directions, respectively. The errors are significantly lower for the TSX Spotlight imagery than for the Stripmap imagery, and the errors are also consistently lower for the range offsets than for the azimuth offsets. In all cases, both range and azimuth error values are an order of magnitude lower than the total accumulated landslide displacement.

To assess offset errors from the natural terrain, areas of land adjacent to the corner reflector points were used to carry out the same analysis. Table 2 shows that the RMS errors for the two offset pairs from natural terrain are at least 20 times higher than from the corner reflector points and are the same order of magnitude as the recorded landslide movements, which therefore suggests natural terrain areas of dense vegetation are not optimal for generating reliable offset measurements in the Three Gorges region. Regardless of the displacement magnitude, corner reflectors remain beneficial for generating precise, 2-dimensional sub-pixel offset measurements only using the SAR amplitude data. Envisat data failed to produce successful offset results given its significantly larger pixel spacing covering the relatively small landslide area. A far greater contrast in the ground terrain backscatter, much faster ground movements or consistent movements over a larger area would all increase

Table 2
Comparison between two independent offset calculations from two image pairs significantly overlapping in time (the first two images in August were used as the two master images, with the last two available images used as the respective slave images). This can help assess the errors between different SAR image modes and also between the offsets calculated from corner reflectors and densely vegetated terrain (directly adjacent to the corner reflector points).

	Range offsets		Azimuth offsets	
Sensor/image mode	Mean difference (m)	RMS error (m)	Mean difference (m)	RMS error (m)
TSX Spotlight (corner reflectors)	0.008	0.011	0.055	0.060
TSX Stripmap (corner reflectors)	0.040	0.038	0.059	0.071
TSX Spotlight (vegetated terrain)	0.574	0.912	1.146	1.478
TSX Stripmap (vegetated terrain)	1.198	1.394	3.044	3.979

the likelihood of obtaining reliable SPOT results from natural terrain in all image modes.

6. Discussion

The movements of the Shuping landslide in May–June 2009, revealed by the SPOT-CR results, demonstrate how the spatial displacement gradient assumption is broken and invalidates long-term D-InSAR analyses. It would be impossible to accurately unwrap any interferogram which spanned this movement episode (without the use of in-situ data) and this issue can perhaps explain the variety of D-InSAR measurements of the Shuping landslide outlined in Section 3. Certainly this time-period should not be analysed using D-InSAR time-series analyses since an even sparser network of measurements (relative to the original interferograms) generated from any form of persistent scatterer interferometry would be less able to resolve such spatially variable measurements.

The SPOT-CR technique is robust when applied to corner reflectors, although it is limited by the rate of movement in relation to the pixel spacing of the SAR data, size of the search window used in the cross-correlation calculation and any significant change in the surface reflectance between image acquisitions. With the use of highly contrasting ground features (i.e. installed corner reflectors in this case), verifiable offset measurements were generated from TSX Spotlight and TSX Stripmap data. When such point-like targets exist over a landslide, it would be beneficial to run SPOT-CR analysis for a stack of SAR images prior to any D-InSAR analysis to assess if any movements exceed the spatial displacement gradient.

Identified as an ancient landslide (Wang, Zhang, et al., 2008), the Shuping landslide is underlain by sandy mudstones and muddy sandstones of the Triassic Badong Formation, a unit within which many landslides are concentrated (Wen, Wang, Wang, & Zhang, 2004). This landslide has been divided into two parts: eastern and western blocks with a combined width of about 600 m. A borehole towards the lower part of Block-1 (eastern) indicated the surface of the rupture zone was at a depth of 65 and 75 m, a zone where numerous slickensides were evident (Wang et al., 2005).

Whilst the rates of displacement are different over the landslide body, the timing of faster and slower episodes (Fig. 7) is very consistent which suggests the same causal factors are affecting the whole landslide. Another capability of sub-pixel offset measurements is the ability to estimate the displacement vectors from the range and azimuth directions to resolve the purely northwards (d_N) and vertical (d_U) components of displacement (Fialko, Simons, & Agnew, 2001). This derivation assumes that landslide movement in the east–west direction (d_E) is zero which is a relatively safe assumption given the orientation of the Shuping landslide with respect to the SAR sensor:

$$\begin{aligned} d_{\text{RANGE}} &= [-0.68 \quad 0.12 \quad -0.72][d_E \quad d_N \quad d_U]^T \\ d_{\text{AZIMUTH}} &= [-0.17 \quad 0.98 \quad 0][d_E \quad d_N \quad d_U]^T \\ d_E &= 0 \end{aligned}.$$

By solving this system of equations, Fig. 8 shows the estimated accumulated vertical and horizontal components of displacement for the Shuping landslide between 21st Feb 2009 and 15th April 2010. A clear topographic trend is visible for the vertical measurements with the total accumulated displacement increasing with elevation. The head of the landslide moved downwards at least 25 times more than the toe of the landslide. The northwards displacement data does not show this trend, but has the greatest movements towards the middle and toe of the landslide. A rotational failure mechanism along a curved plane would be consistent with these 2-dimensional movements and is proposed as a first-order interpretation of the data.

Additionally, the period of most rapid displacement around May–June 2009 corresponds to the annual lowering of the Three Gorges Reservoir (Fig. 9) which accommodates the heavy summer rainfall and helps prevent flooding downstream. The faster the rate of change in the reservoir level, the longer the water table levels take to adjust. When the water-level is lowered, drainage of the landslide lags the reservoir drop which results in high hydraulic gradients and favours slope instability (Shimei, Huawei, Yeming, & Jun, 2008). The biggest displacements appear to correspond to the greatest rates of reservoir lowering, whilst periods of slower reservoir lowering do not lead to an increased propensity of slope failure. However, both the managed and natural changes in the reservoir water-level are related to the seasonal variations in rainfall, so an analysis of landslide movement in relation to both factors is required to fully understand the mechanisms of movement for the Shuping landslide. Corroboration from the analysis of other nearby landslide sites is a subsequent stage of this work.

7. Conclusions

Recognising that landslides often exhibit non-linear and complex displacement patterns, this paper assesses the capability of various SAR image modes (TSX Spotlight, TSX Stripmap and Envisat data) to reliably identify, map, monitor and characterise landslide movement using D-InSAR and a Sub-Pixel Offset Time-series technique applied to corner reflectors (SPOT-CR). The Shuping landslide within the densely vegetated Three Gorges region (China) is used to test these methods on account of the data availability from numerous SAR image modes

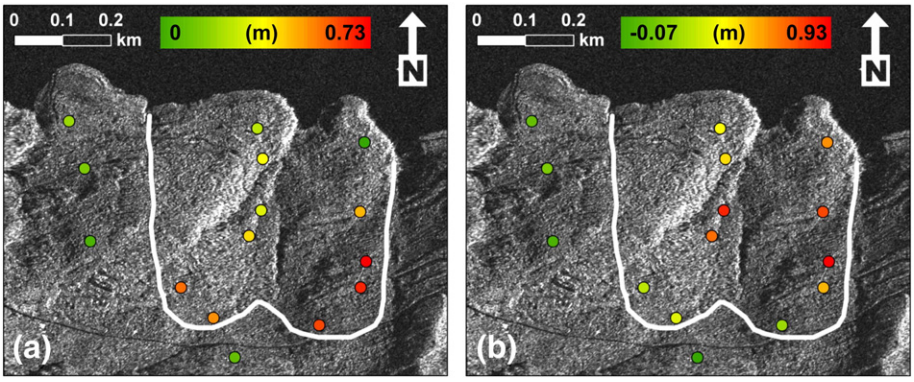

Fig. 8. Using the azimuth and range offset corner reflector measurements (calculated from the first and last TSX Spotlight images), the displacement vectors can be decomposed to calculate the total accumulated vertical (a) and (b) northwards displacement between 21st Feb 2009 and 15th April 2010. The exact values can be found in Supplementary material (Table S3).

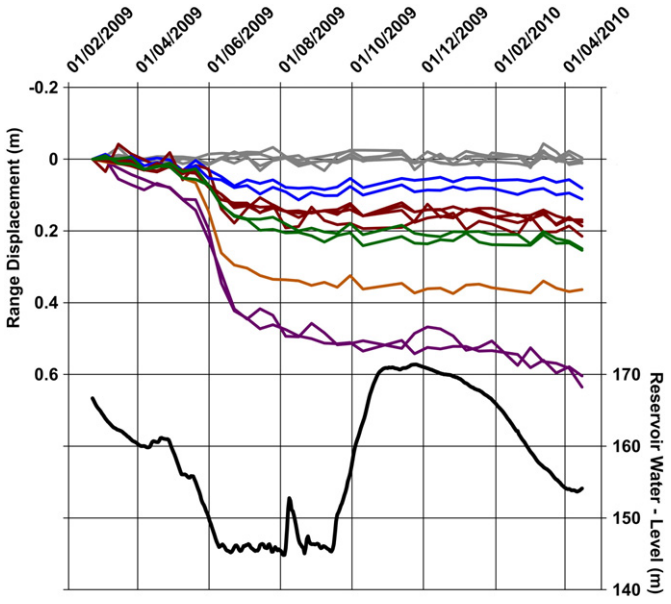

Fig. 9. Range displacement from TSX Spotlight in relation to the water-level changes of the Three Gorges Reservoir.

and the network of corner reflectors installed in and around the landslide body.

D-InSAR measurements can be successfully used to detect movements of the Shuping landslide, although there are significant limitations that prohibit long term D-InSAR monitoring using single-pair and time-series techniques. Interferometric coherence in the Three Gorges region is always low due to the density of vegetation and the limited satellite revisit times, but there are seasonal signals (Fig. 2) most likely caused by consistent annual variations in rainfall and soil moisture. Particularly for TSX imaging modes, it is found that the coherence is highest between November and February each year when rainfall and vegetation coverage is at a minimum.

Despite the problems of low coherence, landslides can be reliably identified and mapped using high resolution D-InSAR measurements providing the movement does not exceed the spatial displacement gradient. However, episodic and faster landslide movements can exceed the displacement gradient (most likely around landslide boundaries) due to the potentially high contrast in displacement rates between stable and moving land (Fig. 3). High displacement gradients identified for the Shuping landslide invalidate the use of D-InSAR time-series approaches for the data stacks from all three SAR image modes used in this study.

Subsequently, a Sub-Pixel Offset Time-series approach applied to corner reflectors is used as a robust method to resolve time-varying landslide displacements. A quantitative, heuristic approach shows how the distribution of offset values for a stable reference area close to the landslide can help reduce the likelihood of spurious correlation and after considering the pixel spacing of SAR data as well as the expected movement of the phenomenon under study, enables suitable sub-pixel offset parameters to be selected (Fig. 4). Additionally the same initial master image is chosen to calculate the displacement time-series from subsequent slave images in order to avoid the propagation of errors associated with an accumulative time-series curve from time-adjacent image pairs. Given the small range in TSX perpendicular baselines (Fig. 6), the use of a small baseline approach for generating time-series displacement curves was not pursued.

Offset measurements from corner reflectors are shown to generate verifiable cross-correlations when located amongst dense vegetation (Fig. 5) and Table 2 shows the errors associated with the corner reflector offsets from TSX data are at least an order of magnitude lower than the landslide displacements. It is also clear that higher resolution SAR data reduces the offset errors.

From the final SPOT-CR analysis, it is clear that large, episodic movements are responsible for a loss of interferometric coherence and the range offset displacement in May 2009 towards the head of the Shuping landslide (Fig. 7) is shown to exceed the displacement gradient measurable by D-InSAR. Assuming the E–W component of displacement is zero, the range and azimuth offsets can be decomposed into estimates of the vertical and horizontal measurements (Fig. 8) to help infer a rotational component of the Shuping landslide and differences between the eastern and western sides of the landslide imply the movements are highly variable and not moving in a uniform manner. Finally, the main episodes of landslide movement appear to occur at the same time as the rapid drawdown of the Three Gorges Reservoir in May/June 2009 (Fig. 9).

This study has considered one landslide in a specific type of terrain. Landslides with different surface features, orientated differently with respect to the SAR sensor and with different movement behaviours, may require different forms of analysis. Areas with less vegetation (either with more buildings or bare rock) which move at slower rates may be more successfully monitored using D-InSAR time series techniques. Larger landslides with displacements spread over a bigger area or moving less episodically would also be more suited for D-InSAR time series analysis. SPOT techniques should achieve better results for landslides with more contrasting surface features (natural or man-made) or where the movement is greater with respect to the SAR image pixel size, up to the point when movement induces significant change in the Earth's surface (and therefore change in the radar backscatter). The application of SPOT techniques to more landslide sites using different SAR data types should be the focus of future studies, and the use of time-adjacent (or small baseline) pairs may be optimal for extracting time-series data from areas of lower correlation. Independent verification of the SAR-derived displacements for the CRs should also be conducted once such data becomes available along with comparing the observed displacement patterns of the Shuping landslide to potential causal factors such as rainfall, groundwater and reservoir water-levels.

Acknowledgements

This work is supported by an EPSRC Industrial Studentship to AS (EP/P505534/1). Part of this work was supported by the Natural Environment Research Council (NERC) through the National Centre for Earth Observation (NCEO), of which the Centre for the Observation and Modelling of Earthquakes, Volcanoes and Tectonics (COMET+) is part. The Envisat images were supplied through the ESA–MOST Dragon 2 Cooperation Programme (ID: 5343). The TSX Spotlight and Stripmap images were supplied through DLR project (ID: GEO0112). We are very grateful to Xiao Cheng for the MET rainfall data from Badong as well as Prof. Simon Wheeler from the University of Glasgow for discussions on the landslide mechanism.

Appendix A. Supplementary data

Supplementary data to this article can be found online at http://dx.doi.org/10.1016/j.rse.2014.03.003.

References

Ahmed, R., Siqueira, P., Hensley, S., Chapman, B., & Bergen, K. (2011). A survey of temporal decorrelation from spaceborne L-band repeat-pass InSAR. *Remote Sensing of Environment, 115*, 2887–2896.

Akbarimehr, M., Motagh, M., & Haghshenas-Haghighi, M. (2013). Slope stability assessment of the Sarcheshmeh landslide, northeast Iran, investigated using InSAR and GPS observations. *Remote Sensing, 5*, 3681–3700.

Baran, I., Stewart, M., & Claessens, S. (2005). A new functional model for determining minimum and maximum detectable deformation gradient resolved by satellite

radar interferometry. *IEEE Transactions on Geoscience and Remote Sensing*, *43*, 675–682.
Bechor, N.B.D., & Zebker, H. A. (2006). Measuring two-dimensional movements using a single InSAR pair. *Geophysical Research Letters*, *33*, L16311.
Berardino, P., Costantini, M., Franceschetti, G., Iodice, A., Pietranera, L., & Rizzo, V. (2003). Use of differential SAR interferometry in monitoring and modelling large slope instability at Maratea (Basilicata, Italy). *Engineering Geology*, *68*, 31–51.
Berardino, P., Fornaro, G., Lanari, R., & Sansosti, E. (2002). A new algorithm for surface deformation monitoring based on small baseline differential SAR interferograms. *IEEE Transactions on Geoscience and Remote Sensing*, *40*, 2375–2383.
Cascini, L., Fornaro, G., & Peduto, D. (2010). Advanced low- and full-resolution DInSAR map generation for slow-moving landslide analysis at different scales. *Engineering Geology*, *112*, 29–42.
Cascini, L., Peduto, D., Pisciotta, G., Arena, L., Ferlisi, S., & Fornaro, G. (2013). The combination of DInSAR and facility damage data for the updating of slow-moving landslide inventory maps at medium scale. *Natural Hazards and Earth System Sciences*, *13*, 1527–1549.
Casu, F., Manconi, A., Pepe, A., & Lanari, R. (2011). Deformation time-series generation in areas characterized by large displacement dynamics: The SAR amplitude pixel-offset SBAS technique. *IEEE Transactions on Geoscience and Remote Sensing*, *49*, 2752–2763.
Colesanti, C., & Wasowski, J. (2006). Investigating landslides with space-borne Synthetic Aperture Radar (SAR) interferometry. *Engineering Geology*, *88*, 173–199.
Cruden, D.M., & Varnes, D. J. (1996). Landslide types and processes. In A. K. Turner, & R. L. Shuster (Eds.), *Landslides: Investigation and mitigation* (pp. 36–75). Washington, DC: Transport Research Board, National Research Council.
Debella-Gilo, M., & Kääb, A. (2011). Sub-pixel precision image matching for measuring surface displacements on mass movements using normalized cross-correlation. *Remote Sensing of Environment*, *115*, 130–142.
Delacourt, C., Allemand, P., Casson, B., & Vadon, H. (2004). Velocity field of the "La Clapière" landslide measured by the correlation of aerial and QuickBird satellite images. *Geophysical Research Letters*, *31*, L15619.
Dzikiti, S., Verreynne, S. J., Stuckens, J., Strever, A., Verstraeten, W. W., Swennen, R., et al. (2011). Seasonal variation in canopy reflectance and its application to determine the water status and water use by citrus trees in the Western Cape, South Africa. *Agricultural and Forest Meteorology*, *151*, 1035–1044.
Ferretti, A., Prati, C., & Rocca, F. (2001). Permanent scatterers in SAR interferometry. *IEEE Transactions on Geoscience and Remote Sensing*, *39*, 8–20.
Fialko, Y., Simons, M., & Agnew, D. (2001). The complete (3-D) surface displacement field in the epicentral area of the 1999 Mw 7.1 Hector Mine earthquake, California, from space geodetic observations. *Geophysical Research Letters*, *28*, 3063–3066.
Foster, J., Kealy, J., Cherubini, T., Businger, S., Lu, Z., & Murphy, M. (2013). The utility of atmospheric analyses for the mitigation of artifacts in InSAR. *Journal of Geophysical Research — Solid Earth*, *118*, 748–758.
Fruneau, B., Achache, J., & Delacourt, C. (1996). Observation and modelling of the Saint-Étienne-de-Tinée landslide using SAR interferometry. *Tectonophysics*, *265*, 181–190.
Fu, W., Guo, H., Tian, Q., & Guo, X. (2010). Landslide monitoring by corner reflectors differential interferometry SAR. *International Journal of Remote Sensing*, *31*, 6387–6400.
Funning, G. J., Parsons, B., Wright, T. J., Jackson, J. A., & Fielding, E. J. (2005). Surface displacements and source parameters of the 2003 Bam (Iran) earthquake from Envisat advanced Synthetic Aperture Radar imagery. *Journal of Geophysical Research — Solid Earth*, *110*, B09406.
Gatelli, F., Guamieri, A.M., Parizzi, F., Pasquali, P., Prati, C., & Rocca, F. (1994). The wavenumber shift in SAR interferometry. *IEEE Transactions on Geoscience and Remote Sensing*, *32*, 855–865.
Goldstein, R. M., & Werner, C. L. (1998). Radar interferogram filtering for geophysical applications. *Geophysical Research Letters*, *25*, 4035–4038.
Haug, T., Kääb, A., & Skvarca, P. (2010). Monitoring ice shelf velocities from repeat MODIS and Landsat data — A method study on the Larsen C ice shelf, Antarctic Peninsula, and 10 other ice shelves around Antarctica. *The Cryosphere*, *4*, 161–178.
Hilley, G. E., Bürgmann, R., Ferretti, A., Novali, F., & Rocca, F. (2004). Dynamics of slow-moving landslides from permanent scatterer analysis. *Science*, *304*, 1952–1955.
Hooper, A. (2008). A multi-temporal InSAR method incorporating both persistent scatterer and small baseline approaches. *Geophysical Research Letters*, *35*, L16302.
Hooper, A., Segall, P., & Zebker, H. (2007). Persistent scatterer interferometric Synthetic Aperture Radar for crustal deformation analysis, with application to Volcán Alcedo, Galápagos. *Journal of Geophysical Research — Solid Earth*, *112*, B07407.
Jiang, M., Li, Z. W., Ding, X. L., Zhu, J. J., & Feng, G. C, (2011). Modeling minimum and maximum detectable deformation gradients of interferometric SAR measurements. *International Journal of Applied Earth Observation and Geoinformation*, *13*(5), 766–777.
Jónsson, S., Zebker, H., Segall, P., & Amelung, F. (2002). Fault slip distribution of the 1999 Mw 7.1 Hector Mine, California, earthquake, estimated from satellite radar and GPS measurements. *Bulletin of the Seismological Society of America*, *92*, 1377–1389.
Kääb, A. (2002). Monitoring high-mountain terrain deformation from repeated air- and spaceborne optical data: Examples using digital aerial imagery and ASTER data. *ISPRS Journal of Photogrammetry and Remote Sensing*, *57*, 39–52.
Leprince, S., Berthier, E., Ayoub, F., Delacourt, C., & Avouac, J. -P. (2008). Monitoring earth surface dynamics with optical imagery. *Eos, Transactions American Geophysical Union*, *89*, 1–2.
Li, Z., Elliott, J. R., Feng, W., Jackson, J. A., Parsons, B. E., & Walters, R. J. (2011). The 2010 MW 6.8 Yushu (Qinghai, China) earthquake: Constraints provided by InSAR and body wave seismology. *Journal of Geophysical Research — Solid Earth*, *116*, B10302.
Li, Z., Fielding, E. J., Cross, P., & Muller, J. -P. (2006). Interferometric Synthetic Aperture Radar atmospheric correction: GPS topography-dependent turbulence model. *Journal of Geophysical Research — Solid Earth*, *111*, B02404.
Li, X., Muller, J. -P., Chen, F., & Yonghong, Z. (2011). Measuring displacement field from TerraSAR-X amplitude images by subpixel correlation: An application to the landslide in Shuping, Three Gorges area. *Acta Petrologica Sinica*, *27*, 3843–3850.
Li, Z., Muller, J. -P., Cross, P., & Fielding, E. J. (2005). Interferometric Synthetic Aperture Radar (InSAR) atmospheric correction: GPS, moderate resolution imaging spectroradiometer (MODIS), and InSAR integration. *Journal of Geophysical Research — Solid Earth*, *110*, B03410.
Li, P., Shi, C., Li, Z., Muller, J. -P., Drummond, J., Li, X., et al. (2012). Evaluation of ASTER GDEM using GPS benchmarks and SRTM in China. *International Journal of Remote Sensing*, *34*, 1744–1771.
Liao, M., Tang, J., Wang, T., Balz, T., & Zhang, L. (2012). Landslide monitoring with high-resolution SAR data in the Three Gorges region. *Science China Earth Sciences*, *55*, 590–601.
Liao, M., Zhang, L., & Balz, T. (2013). Landslide monitoring with high-resolution TerraSAR-X data in the Three Gorges area. *5th TerraSAR-X Science Team Meeting. DLR Oberpfaffenhofen*.
Liu, J. G., Mason, P. J., Clerici, N., Chen, S., Davis, A., Miao, F., et al. (2004). Landslide hazard assessment in the Three Gorges area of the Yangtze River using ASTER imagery: Zigui–Badong. *Geomorphology*, *61*, 171–187.
Massonnet, D., & Feigl, K. L. (1998). Radar interferometry and its application to changes in the Earth's surface. *Reviews of Geophysics*, *36*, 441–500.
Michel, R., Avouac, J. -P., & Taboury, J. (1999). Measuring ground displacements from SAR amplitude images: Application to the Landers Earthquake. *Geophysical Research Letters*, *26*, 875–878.
Onn, F., & Zebker, H. A. (2006). Correction for interferometric Synthetic Aperture Radar atmospheric phase artifacts using time series of zenith wet delay observations from a GPS network. *Journal of Geophysical Research — Solid Earth*, *111*.
Pathier, E., Fielding, E. J., Wright, T. J., Walker, R., Parsons, B. E., & Hensley, S. (2006). Displacement field and slip distribution of the 2005 Kashmir earthquake from SAR imagery. *Geophysical Research Letters*, *33*, L20310.
Peduto, D., Cascini, L., & Fornaro, G. (2010). Satellite radar. In V. Tofani, S. Segoni, F. Catani, & N. Casagli (Eds.), *Evaluation report on innovative monitoring and remote sensing methods and future technology* (pp. 42–43). Oslo: Norwegian Geotechnical Institute.
Quincey, D. J., Lucas, R. M., Richardson, S. D., Glasser, N. F., Hambrey, M. J., & Reynolds, J. M. (2005). Optical remote sensing techniques in high-mountain environments: Application to glacial hazards. *Progress in Physical Geography*, *29*, 475–505.
Rott, H. (2009). Advances in interferometric Synthetic Aperture Radar (InSAR) in earth system science. *Progress in Physical Geography*, *33*, 769–791.
Rott, H., & Nagler, T. (2006). The contribution of radar interferometry to the assessment of landslide hazards. *Advances in Space Research*, *37*, 710–719.
Rott, H., Scheuchl, B., Siegel, A., & Grasemann, B. (1999). Monitoring very slow slope movements by means of SAR interferometry: A case study from a mass waste above a reservoir in the Ötztal Alps, Austria. *Geophysical Research Letters*, *26*, 1629–1632.
SARMAP (2012). *SARScape: Technical description*. Switzerland: SARMAP.
Sassa, K., Picarelli, L., & Yueping, Y. (2009). Monitoring, prediction and early warning. In K. Sassa, & P. Canuti (Eds.), *Landslides — Disaster risk reduction* (pp. 351–375). Berlin, Heidelberg: Springer.
Scambos, T. A., Dutkiewicz, M. J., Wilson, J. C., & Bindschadler, R. A. (1992). Application of image cross-correlation to the measurement of glacier velocity using satellite image data. *Remote Sensing of Environment*, *42*, 177–186.
Shimei, W., Huawei, Z., Yeming, Z., & Jun, Z. (2008). *Back analysis of unsaturated parameters and numerical seepage simulation of the Shuping landslide in Three Gorges Reservoir area.* Landslides and engineered slopes. From the past to the future, two volumes + CD-ROM. CRC Press, 985–990.
Smith, L. C. (2002). Emerging applications of interferometric Synthetic Aperture Radar (InSAR) in geomorphology and hydrology. *Annals of the Association of American Geographers*, *92*, 385–398.
Spagnolini, U. (1995). 2-D phase unwrapping and instantaneous frequency estimation. *IEEE Transactions on Geoscience and Remote Sensing*, *33*, 579–589.
Strozzi, T., Farina, P., Corsini, A., Ambrosi, C., Thüring, M., Zilger, J., et al. (2005). Survey and monitoring of landslide displacements by means of L-band satellite SAR interferometry. *Landslides*, *2*, 193–201.
Stumpf, A., Kerle, N., & Malet, J. -P. (2010). Guidelines for the selection of appropriate remote sensing technologies for monitoring different types of landslides. In A. Stumpf, N. Kerle, & J. -P. Malet (Eds.), *The Deliverable 4.4 of the European SAFELAND Project*.
Tofani, V., Raspini, F., Catani, F., & Casagli, N. (2013). Persistent scatterer interferometry (PSI) technique for landslide characterization and monitoring. *Remote Sensing*, *5*, 1045–1065.
Tofani, V., Segoni, S., Catani, F., & Casagli, N. (2010). Evaluation report on innovative monitoring and remote sensing methods and future technology. In V. Tofani, S. Segoni, F. Catani, & N. Casagli (Eds.), *The Deliverable 4.5 of the European SAFELAND Project*.
Tolomei, C., Taramelli, A., Moro, M., Saroli, M., Aringoli, D., & Salvi, S. (2013). Analysis of the deep-seated gravitational slope deformations over Mt. Frascare (Central Italy) with geomorphological assessment and DInSAR approaches. *Geomorphology*, *201*, 281–292.
Touzi, R., Lopes, A., Bruniquel, J., & Vachon, P. W. (1999). Coherence estimation for SAR imagery. *IEEE Transactions on Geoscience and Remote Sensing*, *37*, 135–149.
UN-ISDR (Ed.). (2004). *Terminology: Basic terms of disaster risk reduction*. Geneva: United Nations.
Wang, H., Harvey, A.M., Xie, S., Kuang, M., & Chen, Z. (2008). Tributary-junction fans of China's Yangtze Three-Gorges Valley: Morphological implications. *Geomorphology*, *100*, 131–139.
Wang, F., Wang, G., Sassa, K., Takeuchi, A., Araiba, K., Zhang, Y., et al. (2005). Displacement monitoring and physical exploration on the Shuping landslide reactivated by impoundment of the Three Gorges Reservoir, China. In K. Sassa, H. Fukuoka, F. Wang, & G. Wang (Eds.), *Landslides* (pp. 313–319). Berlin, Heidelberg: Springer.

Wang, F., Yueping, Y., Zhitao, H., Zhang, Y., Wang, G., & Renjie, D. (2013). Slope deformation caused by water-level variation in the Three Gorges Reservoir, China. In K. Sassa, B. Rouhban, S. Briceno, M. McSaveney, & B. He (Eds.), *Landslides: Global risk preparedness* (pp. 227–237). Berlin: Springer.

Wang, F., Zhang, Y., Huo, Z., Peng, X., Araiba, K., & Wang, G. (2008). Movement of the Shuping landslide in the first four years after the initial impoundment of the Three Gorges Dam Reservoir, China. *Landslides*, *5*, 321–329.

Wangensteen, B., Guðmundsson, Á., Eiken, T., Kääb, A., Farbrot, H., & Etzelmüller, B. (2006). Surface displacements and surface age estimates for creeping slope landforms in northern and eastern Iceland using digital photogrammetry. *Geomorphology*, *80*, 59–79.

Wen, B., Wang, S., Wang, E., & Zhang, J. (2004). Characteristics of rapid giant landslides in China. *Landslides*, *1*, 247–261.

Wen-Yen, C., Chih-Tien, W., Chih-Yuan, C., & Jyun-Ru, K. (2012). Mapping geo-hazard by satellite radar interferometry. *Proceedings of the IEEE*, *100*, 2835–2850.

Xia, Y. (2010). Synthetic Aperture Radar interferometry. In G. Xu (Ed.), *Sciences of geodesy (1)* (pp. 415–473). Berlin: Springer.

Yamaguchi, Y., Tanaka, S., Odajima, T., Kamai, T., & Tsuchida, S. (2003). Detection of a landslide movement as geometric misregistration in image matching of SPOT HRV data of two different dates. *International Journal of Remote Sensing*, *24*, 3523–3534.

Yin, Y., Zheng, W., Liu, Y., Zhang, J., & Li, X. (2010). Integration of GPS with InSAR to monitoring of the Jiaju landslide in Sichuan, China. *Landslides*, *7*, 359–365.

Yun, S. -H., Zebker, H., Segall, P., Hooper, A., & Poland, M. (2007). Interferogram formation in the presence of complex and large deformation. *Geophysical Research Letters*, *34*, L12305.

Zebker, H. A., Rosen, P. A., & Hensley, S. (1997). Atmospheric effects in interferometric Synthetic Aperture Radar surface deformation and topographic maps. *Journal of Geophysical Research — Solid Earth*, *102*, 7547–7563.